Agricultural and Forest Meteorology 255 (2018) 68–80

Contents lists available at ScienceDirect

Agricultural and Forest Meteorology

journal homepage: www.elsevier.com/locate/agrformet

Surface-atmosphere exchange in a box: Making the control volume a suitable representation for in-situ observations

Stefan Metzger[a,b,*]

[a] National Ecological Observatory Network, Battelle, 1685 38th Street, Boulder, CO 80301, USA
[b] University of Wisconsin-Madison, Dept. of Atmospheric and Oceanic Sciences, 1225 West Dayton Street, Madison, WI 53706, USA

ARTICLE INFO

Keywords:
Continuity equation
Data assimilation
Eddy-covariance
Energy balance
Environmental response function (ERF)
Location bias
Mass balance
Representativeness
Upscaling
Virtual control volume (VCV)

ABSTRACT

Using the eddy-covariance (EC) method to determine net surface-atmosphere exchange relies on extensive simplifications of the mass balance concept. Among others, it is assumed that the 3-D flux field within a control volume is divergence-free, which is shown to be violated e.g. from large-eddy simulations. To practically evaluate the severity of these assumptions, case studies have monitored the surrounding of an EC tower, so the control volume can be represented more explicitly. Alternatively, diagnostic tests during data processing can be used to subset the EC data for periods that more likely fulfill the underlying assumptions. However, these existing methods are constrained either by their degree of realism, resource demand, temporal coverage, varying spatial representativeness, or combinations thereof.

It is hypothesized that these deficiencies can be overcome by using the environmental response function (ERF) technique: Relating flux observations at very high spatio-temporal resolution to meteorological forcings and surface properties, and utilizing the extracted relationships to map a single, regular and stationary control volume explicitly in 3-D space and time. Here, the novel ERF virtual control volume (VCV) concept and its implications are derived, and Xu et al. (this issue) are presenting its first practical application.

Initial results show that even from a single EC tower, ERF-VCV reduces advective errors by at least one order of magnitude, and incorporates net low-frequency flux contributions. In the same process tower location bias is treated through attaining a fixed-frame, thus equitable and time-invariant representation of the net surface-atmosphere exchange across a target domain. With regard to the frequently observed non-closure of the surface energy balance, this offers the potential for reconciling “spatial heterogeneity” and “storage term” theories. In extension, ERF promises a rectifying observational operator for unbiased model-data comparison, assimilation, and process representation at model grid scale.

1. Introduction

Earth system models of surface-atmosphere interactions, including the carbon, water, and energy cycles, provide key tools for improving our ability to understand and forecast biosphere responses from local to continental scales. This is especially important in the context of global climate change, already resulting in a 0.85 °C ± 0.20 °C increase in mean global temperature (IPCC, 2013), a ~2% increase in mean global precipitation over land (Hulme et al., 1998), and an intensification of the hydrologic cycle (Hayhoe et al., 2006; Huntington, 2006). The National Academy of Sciences (2013) as well as the IPCC (2013) highlight the need for confronting these models with distributed observations, such as those made by the NEON, AmeriFlux, and ICOS flux tower networks.

However, the spatial mismatch between predictions and observations is complicating the model improvement process (Fig. 1). Specifically, the eddy covariance (EC) method, in which the vast majority of flux tower observations are made, relies on extensive simplifications of the mass balance concept, including assumptions of surface homogeneity and constant sample characteristics with time. As a confounding factor, the flux tower measurement footprint represents only a small fraction of the model grid cell, and the location of this fraction changes with time. As a result, EC flux observations are subject to transient location bias (Nappo et al., 1982; Schmid and Lloyd, 1999) and energy imbalance (Foken et al., 2011; Wilson et al., 2002). These biases are each on the order of tens of percent, one order of magnitude larger than typical sensor errors. The question of scale is underlying both of these challenges, but rigorous testing of methods for scaling land-atmosphere exchange to regular areas and periods relevant for

DOI of original article: http://dx.doi.org/10.1016/j.agrformet.2017.10.011
* Correspondence to: National Ecological Observatory Network, Battelle, 1685 38th Street, Boulder, CO 80301, USA.
E-mail address: smetzger@battelleecology.org.

http://dx.doi.org/10.1016/j.agrformet.2017.08.037
Received 26 December 2016; Received in revised form 29 May 2017; Accepted 30 August 2017
Available online 01 December 2017
0168-1923/

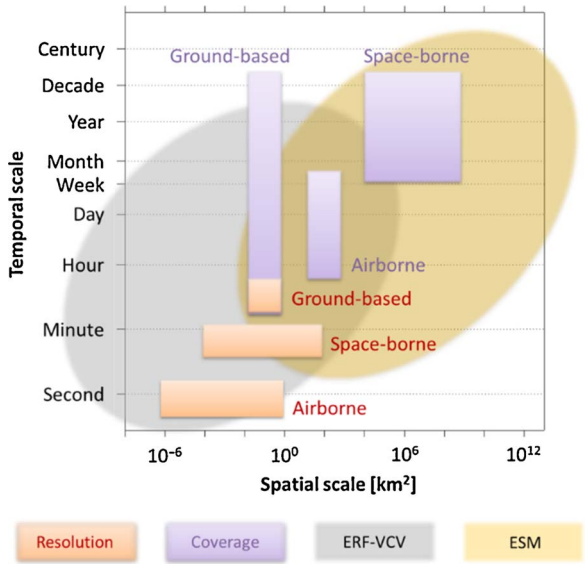

Fig. 1. Space-time scope diagram for a hierarchy of environmental observations in relation to two principal approaches for scaling to an information continuum: Environmental response function virtual control volume (ERF-VCV) and earth system model (ESM).

atmospheric processes and models is limited, and efforts to date have been inconclusive (e.g., Desai et al., 2010).

EC flux tower observations such as those collected by AmeriFlux, ICOS, the forthcoming NEON and the global umbrella network FLUXNET have become available at unprecedented temporal duration and distributed spatial extents: Near continuous data on carbon, water, heat and momentum fluxes and their climate and biological drivers are collected across many eco-climatic domains. The longest running towers are now approaching two decades of observations (Baldocchi, 2008). Significant progress has been made on quality control metrics (Mauder et al., 2013) and addressing systematic biases (Foken et al., 2011). As a consequence, syntheses of flux-tower data have documented age-related changes in carbon flux in forests (Luyssaert et al., 2008), global photosynthetic potential (Beer et al., 2010), global carbon turnover times (Carvalhais et al., 2014), controls of temperature and dryness on latitudinal variations (Yi et al., 2010), and more. However, fundamental challenges remain to adequately integrate EC flux observations into the earth system model improvement process. To date virtually all model-data intercomparisons and regional to global syntheses have neglected uncertainties in EC flux observations resulting from location bias and energy balance non-closure.

These problems are well known, yet unified solutions remain elusive. Desai et al. (2008) significantly improved the comparison between a very tall flux tower and scaled stand-scale flux towers by “de-biasing” the tall tower footprint. Wang et al. (2006) demonstrated retrieval of land cover specific respiration and photosynthesis parameters by utilizing hour-to-hour variations in flux footprint. Overall, location bias diagnostics (Chen et al., 2011; Chen et al., 2012) or corrections (rectification) have been applied only in limited domains.

Solutions to the energy balance closure problem are even less developed: The surface energy balance at most EC sites is not closed, the available energy often 10–30% larger than the sum of the turbulent fluxes (e.g., Stoy et al., 2013; Wilson et al., 2002). Numerous reasons are proposed for the lack of energy balance closure. Recent studies evaluating sensor uncertainty and spatial scaling have ruled out radiation and ground heat measurements as the primary cause (e.g., Horst et al., 2015; Liu et al., 2011). Flawed measurement and interpretation of heat storage in soil, air column, and biomass below the EC measurement has shown promise in reducing the bias (Leuning et al., 2012; Lindroth et al., 2010). However, it does not apply similarly across sites: For example, over low stature ecosystems storage in air and biomass are typically of little relevance. Similarly, horizontal and vertical divergence terms can lead to a lack of closure, but in complex terrain it is difficult to attribute a systematic loss of energy since coupling should occur at least periodically (e.g., Barr et al., 2013; Zitouna-Chebbi et al., 2012). This leaves landscape heterogeneity and associated low-frequency mesoscale circulations (e.g., Foken, 2008; Panin et al., 1998) as suggested systematic source, with the bias largely attributed to simplifications of the mass balance concept upon which most EC studies depend (Finnigan et al., 2003).

To practically evaluate the severity of violated EC assumptions, case studies have monitored the surrounding of an EC tower to more explicitly represent a control volume (incl. storage and divergence terms, Aubinet and Feigenwinter, 2010; Foken et al., 2010; Oncley et al., 2007). Alternatively, diagnostic tests during data processing can be used to subset the EC data for periods that more likely fulfill the underlying assumptions (Foken et al., 2004; Mauder and Foken, 2006). However, these existing methods are constrained either by their degree of realism, resource demand, temporal coverage, varying spatial representativeness, or combinations thereof.

I posit here that surface heterogeneity and changing sample characteristics over time are not problems that necessarily require additional data filtering. Instead, they are characteristics whose inherent variability can be utilized to develop better flux data products for model evaluation, assimilation, and improvement. This shall be achieved through transferring EC flux observations from multiple mismatching, irregular and transient control volumes to a single matching, regular and stationary control volume. It is accomplished by expanding the temporally resolved but planar environmental response function (ERF) technique (Metzger et al., 2013a; Xu et al., 2017) to a virtual control volume (VCV).

The objective of this manuscript is to derive the theoretical background and requirements for ERF-VCV, and thus to provide a means for addressing the location and energy balance biases underlying EC flux measurements. I will test the hypothesis that the resilience of tower eddy-covariance measurements to advection errors can be improved by at least one order of magnitude through combining spectral averaging with source area modeling and spatio-temporally explicit ensembling. In the following sections the ERF-VCV concept and its implications are derived. Section 2 introduces the methodology, beginning from the control volume framework (Section 2.1), and then using ERF-VCV to formally interrelate point measurements to it (Sections. 2.2–2.4). Section 3 presents example results, beginning with performance requirements (Sect. 3.1), then discussing implications of representation and representativeness on energy imbalance (Section 3.2), as well as practical difficulties and proposed solutions (Section 3.3). Section 4 summarizes my findings and provides an outlook. In extension, Xu et al. (this issue) present the first practical application of ERF-VCV.

2. Materials and methods

The exchange of momentum, heat, water vapor, CO_2 and other scalars between the earth’s surface and the atmosphere is often dominated by turbulent transport: Buoyancy as well as shear stress result in a turbulent wind field for most of the day (e.g., Stull, 1988). The EC technique utilizes these turbulence properties, making it a suitable method for the direct and continuous monitoring of surface-atmosphere interactions. However, questions arise from inherent theoretical assumptions of the EC method about relevant terms to the full mass balance, spatial scale and representativeness, and energy balance closure. All of these impact environmental inference and the efforts to develop and test model parameterizations.

In the following I will explore the foundation of EC, the formal control volume framework (Section 2.1). This is followed by deriving ERF-VCV, through relating point measurements to surface patches (Section 2.2), and subsequently surface patches to the control volume (Section 2.3). Section 2.4 provides the minimum requirements for applying ERF-VCV to flux towers.

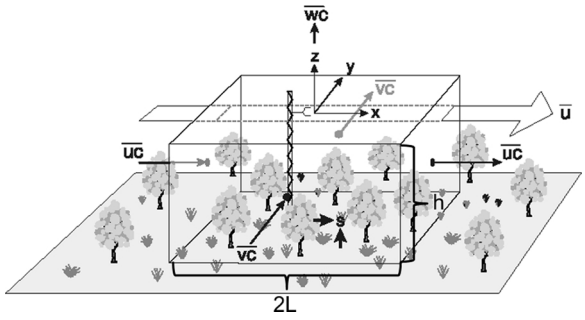

Fig. 2. EC measurements from an Eulerian perspective. Conceptual framework of a regular and stationary control volume, modified after Finnigan (2004).

2.1. The control volume framework

The net exchange between surface and atmosphere (*NSAE*) relies on mass conservation, and can be expressed as the Reynolds decomposition (isolation of mean and fluctuating parts) of relevant terms in the continuity equation (e.g., Foken, 2017; Stull, 1988). Here, c is a scalar quantity such as temperature, H_2O or CO_2 dry mole fractions; u, v and w are wind components with respect to the Cartesian coordinate axes x, y, and z; t is time, and h is the height of the EC measurement located at the lid of the control volume and centered with respect to its length and width 2 L (Fig. 2). The overbars indicate a time average, and primes denote turbulent deviations from the time average:

$$
\begin{aligned}
NSAE = & \int_0^h \left[\frac{1}{4L^2} \int_{-L}^{+L} \int_{-L}^{+L} \frac{\partial \overline{c}}{\partial t} dxdy \right] dz && \text{I} \\
& + \int_0^h \left[\frac{1}{4L^2} \int_{-L}^{+L} \int_{-L}^{+L} \left\{ \frac{\partial \overline{u}\overline{c}}{\partial x} + \frac{\partial \overline{u'c'}}{\partial x} + \frac{\partial \overline{v}\overline{c}}{\partial y} + \frac{\partial \overline{v'c'}}{\partial y} \right\} dxdy \right] dz && \text{II} \\
& + \int_0^h \left[\frac{1}{4L^2} \int_{-L}^{+L} \int_{-L}^{+L} \left\{ \frac{\partial \overline{w}\overline{c}}{\partial z} + \frac{\partial \overline{w'c'}}{\partial z} \right\} dxdy \right] dz. && \text{III}
\end{aligned}
\tag{1}
$$

In Eq. (1) line I represents enrichment or depletion of the scalar within the control volume, i.e. change in storage. Lines II and III represent the sum of advective and turbulent fluxes between the control volume bottom and lid, in the horizontal (line II) and vertical (line III) directions, respectively. Line III differs from Finnigan (2004); Finnigan et al. (2003) in that it retains the vertical differential and integration operators. This property principally supports the vertical partitioning of sources at various heights, such as encountered in multistory ecosystems and urban environments (Section 3.3). Line III reduces to $\frac{1}{4L^2} \int_{-L}^{+L} \int_{-L}^{+L} \{\overline{w}\overline{c}(h) + \overline{w'c'}(h)\} dxdy$ for applications in which only the net exchange is of interest, i.e. the vertical differential and integration operators cancel with $\overline{w}\overline{c}(0) \rightarrow 0$ and $\overline{w'c'}(0) \rightarrow 0$.

In order to quantify the complete mass balance, all of the terms in Eq. (1) should be measured. However, even with a well-equipped EC tower only few terms in Eq. (1) are actually measured, reducing Eq. (1) to Eq. (2): In line I the local storage change is measured along the vertical tower column, in line II horizontal fluxes are not measured at all, and in line III only the local turbulent vertical flux is measured at the tower top. To nevertheless permit a statement about *NSAE*, the control volume is assumed to be horizontally homogeneous (i.e., $\partial/\partial x = 0$, $\partial/\partial y = 0$), thus theoretically cancelling the remaining terms:

$$
\begin{aligned}
NSAE = & \int_0^h \frac{\partial \overline{c}}{\partial t} dz && \text{I} \\
& + 0 && \text{II} \\
& + \overline{w'c'}\ (h). && \text{III}
\end{aligned}
\tag{2}
$$

However, real ecosystems are heterogeneous in many respects and on many scales. Thus, what little is directly measured results in various known complications (Finnigan et al., 2003):

(i) The local storage change measured along the vertical tower column, Eq. (2) line I, is no longer necessarily equal to the storage change across the control volume, Eq. (1) line I.
(ii) The horizontal flux divergence, Eq. (2) line II, is no longer necessarily zero across the control volume, Eq. (1) line II.
(iii) The local turbulent vertical flux measured at the tower top, Eq. (2) line III, is no longer necessarily equal to the turbulent and advective vertical flux integrated across the control volume, Eq. (1) line III.

In short: For determining *NSAE* over non-homogeneous landscapes, Eq. (2) cannot represent the actual control volume mass balance. As a practical workaround, flux observations are often filtered e.g. by stationarity, turbulent mixing and blending height tests for periods that more likely fulfill these assumptions (e.g., Foken and Wichura, 1996; Mahrt, 2000). In the following I will explore a fundamental solution to this long-standing dilemma, i.e. explicitly addressing each term in Eq. (1) through ERF-VCV with data from a single tower and remote sensing alone.

2.2. From points to patches

Conceptually, tower EC measurements attempt to replace a spatial ensemble of instantaneous values at multiple locations with a sufficiently long temporal record at one point: The frozen turbulence similarity theory (Taylor, 1938) provides a convenient approach to the necessary transformation between Eulerian and Lagrangian flow formalisms.

2.2.1. Representation error

The flux footprint concept (Leclerc and Foken, 2014; Schmid, 2002; Vesala et al., 2008) provides a useful illustration of such transformation: The time averaged measurement at one point represents the flux of energy or some atmospheric constituent to or from an upwind surface patch known as the flux footprint, whose area increases with h. At a predefined significance level, the ensemble trajectory of all Lagrangian particles contributing to the measurement can be enveloped by the horizontally footprint-weighted volume below the measurement (Fig. 3). This volume varies over time as a function of vegetation height, canopy roughness, wind direction, shear stress, atmospheric stability, wind variance, and several other factors (Kljun et al., 2015).

The footprint itself can be interpreted as the surface patch to which the mass balance computed at the tower refers (Finnigan, 2004). In consequence, the footprint volume corresponds to the Lagrangian, irregular and transient control volumes our measurements actually observe (Fig. 3). As can be seen, this is in stark contrast to the Eulerian, regular and stationary control volume in Fig. 2, which per Eq. (1) our measurements are formally required to represent. In the following I will refer to this as representation error.

In a homogeneous surface layer, per definition of $\partial/\partial x = 0$, $\partial/\partial y = 0$, the representation error is zero, and our measurements can be used to calculate the mass balance directly via Eq. (2). Over a non-homogeneous landscape, however, the observed flux is subject to random and systematic variations due to changes in the area and volume that is sampled (Fig. 3). This necessitates transforming

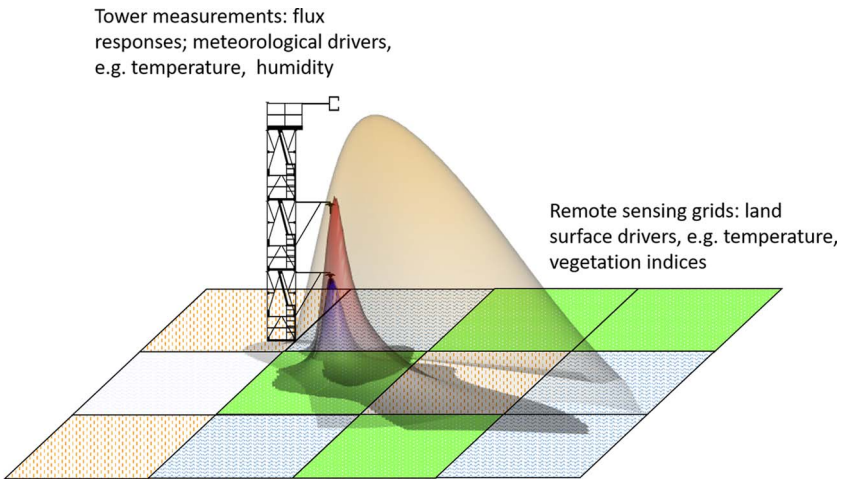

Fig. 3. EC measurements from a Lagrangian perspective. The upwind flux footprint volumes are shown as semi-transparent 3-D envelopes with different colors for each level. ERF-VCV links the tower-measured flux response to in-situ meteorological measurements and footprint-weighted biophysical surface properties.

observations that are best described in a Lagrangian representation to the Eulerian representation required by Eq. (1). The matter is additionally aggravated for the storage change measured along the vertical tower column (Eq. (2) line I), for which each measurement level represents a different, mismatching surface area and thus control volume (Raupach, 1988). To date even sophisticated analyses of the storage term (e.g., Bjorkegren et al., 2015) have yet to address this representation error.

2.2.2. Representativeness error

Representativeness of a measurement is defined as the extent to which it reflects the actual conditions in the space-time domain of interest (Nappo et al., 1982). Any transient bias that occurs from changes in sampled characteristics with time will bias environmental inference and model-data comparison, and thus corrupt the model improvement process. Essentially, observations and modeling currently coexist on two completely different spatial scales, requiring some treatment of the observations to inform models (Fig. 4).

There are currently two basic approaches to bridge this scale gap,

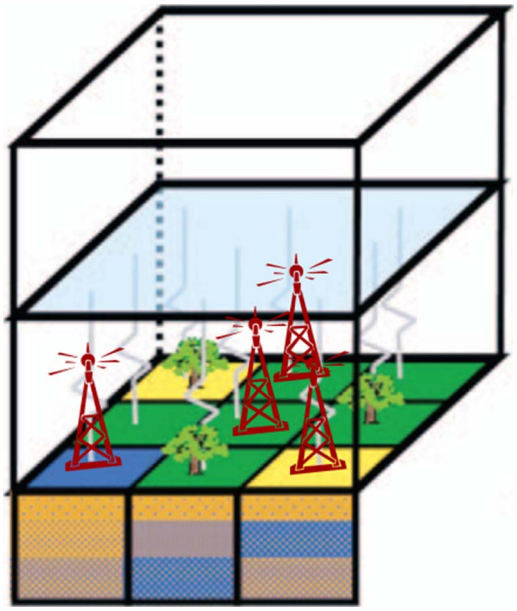

Fig. 4. How well an in-situ measurement can represent a model grid cell depends on its placement in a heterogeneous landscape. Modified after Mengelkamp et al. (2006).

data-driven and process-based. Data-driven approaches minimize assumptions by inferring relationships among observations directly from the available data. A simple example of data-driven methods is the “tile-approach”, which expresses a measured flux as a linear composite of contributing land surface fractions (e.g., Beyrich et al., 2006; Chen et al., 1999; Fig. 4). This approach neglects to account for intra-class variability; however, several studies have shown that even within the same vegetative class different surface areas can dominate the fluxes of different scalars (Bertoldi et al., 2013; Metzger et al., 2013a).

On the other hand, process-based approaches rely on prescribed mechanistic relationships, which are typically valid only for steady-state conditions. One class of algorithms focuses on remotely-sensed properties of the land surface, allowing to determine biases introduced through spatial aggregation (Ershadi et al., 2013; Stoy et al., 2009). Land surface models utilize additional in-situ observations (e.g., Chen et al., 2010; Xiao et al., 2011). A key limitation to process-based approaches is the assumption of energy and water balance closure (e.g., Anderson et al., 2008; Cammalleri et al., 2012), which is not typically achieved from observations in the field.

In the following I will examine how ERF-VCV combines the strengths of data-driven and process-based approaches to address both, representation error and representativeness error.

2.3. From patches to control volume

One major challenge for deciphering the controls of surface-atmosphere exchange lies in the observational co-variations in space (e.g., source attribution) and time (e.g., diel cycle in surface forcing). The ERF-VCV procedure permits the necessary de-convolution and rectification through the systematic and synergistic extraction and re-projection of information. In Section 2.3.1 I will first explore the foundations of ERF-VCV data processing, and then apply it in Section 2.3.2 to reconcile the multiple Lagrangian control volumes into a single Eulerian volume per Eq. (1).

2.3.1. The ERF-VCV technique

ERF-VCV is a progression of the ERF technique (Metzger et al., 2013a) from time-resolved 2-D planar to 3-D cuboid dimensionality. This is achieved through relating flux ‘response’ observations at very high spatio-temporal resolution to meteorological ‘drivers’ and surface properties. The extracted relationships are then used to explicitly re-project fluxes in 3-D space and time throughout the VCV (Fig. 5). These steps are realized by coupling time-frequency-decomposed flux observations with flux footprint modeling and machine learning.

Based on the considerations of isotropy and ergodicity, the

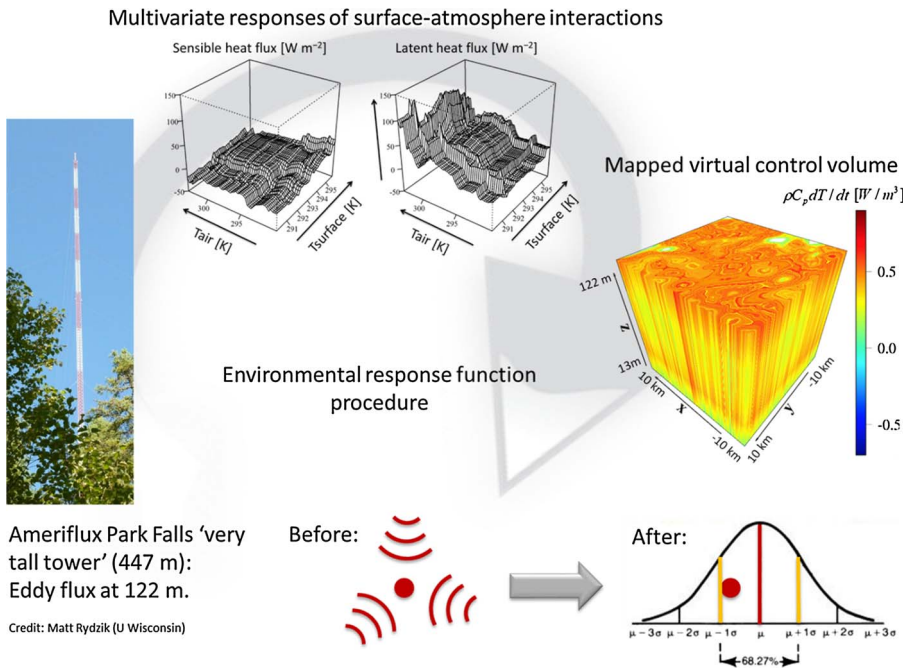

Fig. 5. Essential steps of the ERF procedure, from observation over response function extraction to spatio-temporal projection and resulting spatial probability density function.

traditional EC approach requires averaging turbulent fluctuations at the tower-top over a 15–60-min window depending on measurement height (e.g., Foken, 2017). This makes it susceptible to changing turbulent conditions and source area variations that occur on shorter time scales (Schaller et al., 2017). By using a Wavelet-based spectral average the flux measurement period can be reduced substantially without neglecting long-wavelength flux contributions (order 5-min averages; Charuchittipan et al., 2014). Here, the Morlet mother Wavelet is used, which has been shown to permit clear spatial attribution when used in combination with footprint modeling (Metzger et al., 2013a). Storage time-rate-of-change at multiple measurement heights below the tower-top is determined from the time-differences of 15 min block-averages (Xu et al., this issue).

Meteorological drivers are obtained from temporally continuous in-situ measurements, and surface properties from footprint-weighted spatially continuous remote sensing data products. These two types of drivers complement each other to explain the spatio-temporal variation of the flux responses. Specifically, the utility of meteorological drivers such as potential temperature and water vapor dry mole fraction is to explain temporal variation. They are utilized from observations above the blending height (Mahrt, 1996; Mason, 1988) so that the assumption of spatial homogeneity is weak. In contrast, the utility of biophysical land surface properties such as temperature and vegetation indices is to explain spatial variation. Consequently, remote sensing data products are downscaled linearly in time to daily resolution, and bi-linearly in space to horizontal resolution equaling the EC measurement height (Xu et al., 2017). The biophysical properties in the 'Lagrangian' surface area represented by each observed turbulent flux and storage time-rate-of-change response is determined through flux footprint modeling (Kljun et al., 2004; Metzger et al., 2012) using the Wavelet-based turbulence statistics as inputs (Metzger et al., 2013a; Xu et al., this issue).

The resulting large sample size and high signal-to-noise ratio enables machine learning to extract key relationships between the atmospheric flux responses, and land surface and meteorological drivers. Here, the boosted regression trees technique is used (Elith et al., 2008; Metzger et al., 2013a). In terms of driver selection, temperature and water vapor gradients between surface and atmosphere, solar radiation and relative measurement height within the boundary layer have shown to be important controls on the observed fluxes, incl. vertical flux divergence. To improve the signal/noise ratio, only observations that pass the test sequence after Xu et al. (this issue) are used for machine learning: De-spiking of raw data, periods with excessive missing data, fluxes approaching the detection limit, de-spiking of flux observations, integral turbulence characteristics. The importance of each driver is then determined by how much variation of the response it explains, which together with fundamental process understanding is used to include or drop the driver. Total explained variation is in excess of 95%. Once extracted, the multi-dimensional response function is used alongside the continuously available drivers to re-project the time-resolved flux throughout the 'Eulerian' VCV. The turbulent flux is directly projected to the lid of the Eulerian control volume. In contrast, the storage time-rate-of-change is projected to multiple levels between the control volume surface and lid, and the grid-cell storage flux is then determined from vertical integration.

To summarize, ERF-VCV acts as a solver that catalyzes process and artificial intelligence concepts: It employs well understood process descriptions such as footprint modeling and vertical gradients in combination with non-aligned observations such as from towers, aircrafts and satellites alike. It then mines all the information contained in the provided processes and observations. In result an answer to a complex question is provided incl. confidence intervals, such as the Lagrangian-to-Eulerian transformation of flux observations.

This can be formally expressed with R ($x_{1\ldots X}$, $y_{1\ldots Y}$, $z_{1\ldots Z}$, $t_{1\ldots T}$) being comparatively expensive and sparse response observations, such as those made by EC flux towers. In contrast, driver observations D ($x_{1\ldots X}$, $y_{1\ldots Y}$, $z_{1\ldots Z}$, $t_{1\ldots T}$) are comparatively cheap and collectively dense, such as temperature measurements made by meteorological stations, commercial aircraft and satellite. Together with the existing process understanding P, the ERF extraction is sparse in x, y, z, t − space through dataset R_1:

$$ERF = f(R_1, D_1, P). \quad (3)$$

In contrast, the ERF projection acts as transfer function on dataset D_2, and the resulting R_2 is dense in x, y, z, t – space:

$$ERF(D_2, P) \rightarrow R_2. \quad (4)$$

As such, ERF yields the most complete approximation of the true R_2 that is possible from the provided information. The Lagrangian-to-Eulerian transformation of flux observations is an ERF example

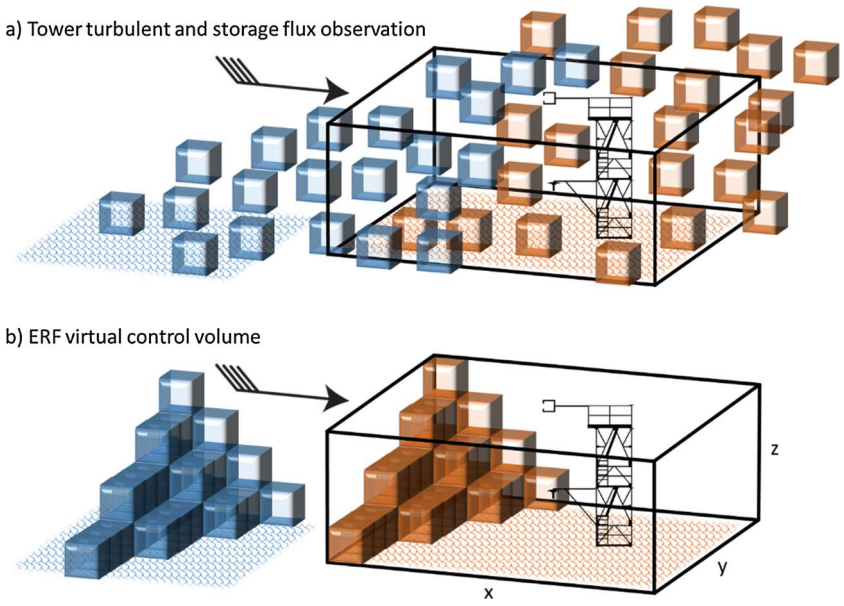

Fig. 6. Tower turbulent and storage flux measurements in a cuboid control volume. Top panel: Tower observations in a "leaky" control volume with air parcels from within and beyond the control volume passing by the tower. Bottom panel: ERF-VCV mapping operator independently considering the surface forcing on an air parcel and its atmospheric mediation, while inhibiting its lateral displacement.

application. The resulting ERF-VCV minimizes methodological assumptions, e.g. no linearity or closure of energy or water balances are required.

2.3.2. Reconciling continuity, representation and representativeness

Although the EC technique assumes homogeneity, real ecosystems are heterogeneous in many respects and on many scales. Superimposing the Lagrangian footprint concept over a Eulerian control volume, this can be visualized as a "leaky box" (Fig. 6 top panel). That is, the tower measures air parcels that partially originate from beyond the boundaries of a homogeneous surface patch. Among others, this fraction depends on measurement height, i.e. the turbulent flux observation on the tower top sources a different ratio of these surface patches compared to the storage term profile observations below. As a practical workaround, flux observations are often filtered e.g. by stationarity tests for periods that more likely fulfill the necessary assumptions.

Here, I propose a solution to this long-standing dilemma, i.e. making a single, regular, stationary and divergence-free control volume an accurate representation for all available in-situ observations (Fig. 6 bottom panel): ERF-VCV provides the necessary 4-D operator to explicitly map all terms in Eq. (1) from tower storage and vertical flux observations. This is achieved by decomposing the flux response into surface forcing (e.g., heat emission, the process of interest) and its atmospheric transport (e.g., blending, the process that complicates interpretation). This allows holding the air parcels horizontally in place within the control volume, thus permitting to focus on the surface forcing, i.e. the quantity of interest. Practically, this is achieved through combining spectral averaging with source area modeling and spatio-temporally explicit ensembling, as detailed in the following.

First, the vertical advection term $\overline{w}\,\overline{c}(h)$ is conveniently included in the total vertical flux $\overline{wc}(h)$, which is achieved through spectral averaging $\overline{w}\,\overline{c}(h) + \overline{w'c'}(h)$ using Wavelets. The approach is similar to Ogives in the frequency domain (Desjardins et al., 1989): Spectral contributions are cumulated from high to low frequencies until $\overline{wc}(h)$ trends to a stable value at the spectral gap between turbulent and diurnal scales. Time-frequency procedures such as Wavelets have the additional advantage that $\overline{wc}(h)$ can be discretized at time resolutions that are much shorter (e.g., minutes) compared to the maximum considered transport scale (e.g., hours; Barnhart et al., 2012; Xu et al., this issue). Here, Wavelet transport scales up to several hours are considered, with flux results discretized at a period of several minutes. Over these transport scales atmospheric motions such as the passage of convective eddies or mesoscale circulations can induce non-zero $\overline{w}$, and compensating horizontal advection and storage in any such period (Finnigan et al., 2003; Mauder et al., 2008). At a single tower, period-to-period variations in $\overline{w}\overline{c}(h)$ may thus greatly exceed $\overline{w'c'}(h)$: $\overline{w}\overline{c}(h)$ carries not only the net low-frequency contribution to the vertical flux, but partially compensates the horizontal flux divergences $\int_0^h \frac{\partial \overline{u}\overline{c}}{\partial x} + \frac{\partial \overline{v}\overline{c}}{\partial y} dz$ which cannot be measured from a single tower. As a result the period-to-period variations of the total vertical flux $\overline{wc}(h)$ are very noisy (Finnigan et al., 2003). The fundamental challenge here is that the net low-frequency flux is masked by the time-varying compensatory flux in the same frequency range but of potentially larger magnitude.

Second, a flux footprint model (Kljun et al., 2004; Metzger et al., 2012) is used to link the observed total flux responses to surface drivers. The utilized footprint model provides a solution to the advection-diffusion equation that assumes horizontally homogeneous turbulence and steady-state. It thus tends to perform better at attributing high-frequency flux contributions to their local sources as compared to attributing compensatory fluxes incl. the net low-frequency flux to their more distant sources. Thus, footprint-weighted land surface drivers are derived with the surface sources of the compensatory fluxes only partially attributed (Metzger et al., 2013a).

Third, machine learning extracts the relationships between 1000s of flux observations and the footprint-weighed land surface drivers as well as meteorological forcings. In this process the ensemble effect over many fragments results in a near-complete reproduction of the high-frequency flux as well as the compensatory fluxes, which are propagated into the resulting response functions.

Fourth, the compensatory fluxes are remedied during machine projection: An ensemble can be created of multiple periods at a single tower in homogenous terrain (Finnigan et al., 2003), or of a single period at multiple distributed towers in heterogeneous terrain (Desai et al., 2016; Engelmann and Bernhofer, 2016; Mauder et al., 2008; Steinfeld et al., 2007). Here I consider the spatial case, for which the horizontal flux divergence $\int_0^h \left[\frac{1}{4L^2} \int_{-L}^{+L} \int_{-L}^{+L} \left\{ \frac{\partial \overline{u}\overline{c}}{\partial x} + \frac{\partial \overline{v}\overline{c}}{\partial y} \right\} dx dy \right] dz$ trends

towards its ensemble value of zero with increasing domain size, thus cancelling Eq. (5) line II. Correspondingly, residual compensatory flux is removed from the storage term $\int_0^h \left[\frac{1}{4L^2} \int_{-L}^{+L} \int_{-L}^{+L} \frac{\partial \overline{c}}{\partial t} dxdy \right] dz$ in Eq. (5) line I, and the vertical advection $\frac{1}{4L^2} \int_{-L}^{+L} \int_{-L}^{+L} \overline{wc}(h) dxdy$ as component of the net vertical flux Eq. (5) line III trends to its net low frequency flux contribution.

$$
\begin{aligned}
NSAE &= \int_0^h \left[\frac{1}{4L^2} \int_{-L}^{+L} \int_{-L}^{+L} \frac{\partial \overline{c}}{\partial t} dxdy \right] \mathrm{dz} && \text{I} \\
&+0 && \text{II} \\
&+ \frac{1}{4L^2} \int_{-L}^{+L} \int_{-L}^{+L} \overline{wc}(h) \mathrm{dxdy}. && \text{III}
\end{aligned}
\tag{5}
$$

To summarize the space and time resolved realization of Eq. (5): ERF-VCV does not assume that the utilized storage and vertical flux observations represent the true surface flux. Rather, it acknowledges that the observations are a combination of the net surface flux and atmospheric dynamics, such as quasi-stationary structures and convective eddies. By means of statistical inversion, ERF-VCV acts as transfer function on the meteorological and surface forcings: The total storage and vertical fluxes are projected into areas with similar surface and meteorological state-space combinations. In result, the tower storage and total vertical flux observations are transferred from their multiple mismatching Lagrangian control volumes into the grid cells of a single matching Eulerian control volume. The resulting flux grids represent the spatial ensemble as it would be observed from one virtual tower in each grid cell: The tower's footprint continuously covers only that cell. The resulting consistent representation along its large number of individual grid cells permits cancellation of the compensation flux components and thus to determine the net surface flux for ensembles of grid cells, e.g. along cross-sections, land covers etc.

Compared to a single flux tower with a transient flux footprint, the ERF-VCV flux field provides continuous information on flux spatial patterning and frequency of occurrence across the entire target domain. It thus permits to extend spatial representativeness from the flux footprint to a model grid-size target domain.

2.4. Minimum requirements for applying ERF-VCV to flux towers

Depending on landscape fragmentation, the VCV side length $2L$ can be expected to be on the order of $50\,h < 2L < 200\,h$, with h being the turbulent flux measurement height. When exceeding this scale, ERF-VCV over heterogeneous terrain has shown to project missing values in > 10% of all cases: The number of driver combinations that are not encountered in the training dataset typically increases with distance from the tower. It should be noted that over homogeneous terrain one should expect the application of ERF-VCV to be obsolete, as standard EC assumptions are theoretically fulfilled. For a minimalistic application of ERF-VCV to sensible and latent heat flux observations (responses), the solar forcing, boundary layer height and vertical gradients of temperature and humidity can be used (drivers). Turbulent sensible and latent heat flux observations at the tower top should be accompanied by profile observations of temperature and humidity to determine the corresponding storage fluxes. Several options are available for providing driver information, incl. proxy information. For example, the solar forcing can be expressed as observed net radiation (Metzger et al., 2013a), but also via the solar azimuth angle (Xu et al., this issue). Analogously, boundary layer height can be provided from Ceilometer or similar measurements, or re-analysis data. The gradients of temperature and humidity are easily constructed in the ERF by providing air temperature and humidity observations, and corresponding land surface proxies such as MODIS land surface temperature and vegetation indices (Metzger et al., 2013a; Xu et al., this issue). To keep the assumption of spatial homogeneity weak, the air temperature and humidity observations should be taken from a tower level above the blending height. Similarly, the spatial resolution of the land surface drivers should be on the order of h or finer to enable sufficient spatial attribution. Applying ERF-VCV to observations that fall short of these requirements is principally possible. However, the resulting uncertainties warrant careful investigation.

The ERF-VCV routines were developed in GNU R version 3.1 (R Core Team, 2016) as part of the eddy4R family of R-packages (Metzger et al., 2017; Xu et al., this issue). Corresponding Docker compute images, R-packages and workflow examples are being developed for a public repository, and are available upon request at the time of writing.

The ERF-VCV analysis required ~130 CPU-minutes and ~10 GB memory per 24 h of 20 Hz turbulence data, 1 Hz profile data with 2 observation levels and 5 projection levels, and 2 land surface drivers over a 200 × 200 cell grid. The input data size (gzip or hdf5 compressed) is ~0.5 GB, machine learning requires ~10 CPU-minutes and 2 GB memory, and machine projection requires ~120 CPU-minutes and 10 GB memory. The output data size is < 0.1 GB per day. For successful application ERV-VCV requires several weeks of data. For this purpose it is possible to parallelize ERV-VCV over multiple CPUs.

3. Results and discussion

In the following I investigate the hypothesis that ERF-VCV can improve the resilience of tower EC measurements to advection errors by at least one order of magnitude. Corresponding performance requirements on a suitable data analysis tool are derived in Section 3.1. This is followed by example results in Section 3.2, which are used to illustrate the utility of ERF-VCV for addressing EC location and energy balance biases. Lastly, Section 3.3 discusses remaining practical difficulties and proposed solutions.

3.1. Performance requirements

ERF-VCV sets out to reduce EC advection errors through combining spectral averaging with source area modeling and spatio-temporally explicit ensembling. The individual utility, performance and limitations of spectral averaging (e.g., Charuchittipan et al., 2014; Schaller et al., 2017; Strunin and Hiyama, 2004; Thomas and Foken, 2005; van den Kroonenberg and Bange, 2007) and source area modeling (Kljun et al., 2015; Leclerc and Foken, 2014; Markkanen et al., 2010; Rannik et al., 2012; Vesala et al., 2008) are well documented. In their uncertainty budgets Xu et al. (2017) and Metzger et al. (2013a) determine their combined effects on the ERF results to 0–4% bias and 1–5% standard error depending on the number of aggregated grid cells.

This points to the possibility of using spatio-temporally explicit

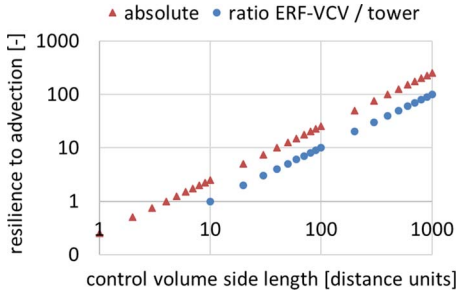

Fig. 7. Resilience of EC tower measurements and ERF-VCV net surface flux maps to external advection errors. Black boxes indicate the typical ranges of EC tower and ERF-VCV, respectively. The red triangles represent the absolute resilience calculated as ratio of explained to unexplained surfaces of an Eulerian control volume, and the blue circles represent the resilience of ERF-VCV relative to the EC tower.

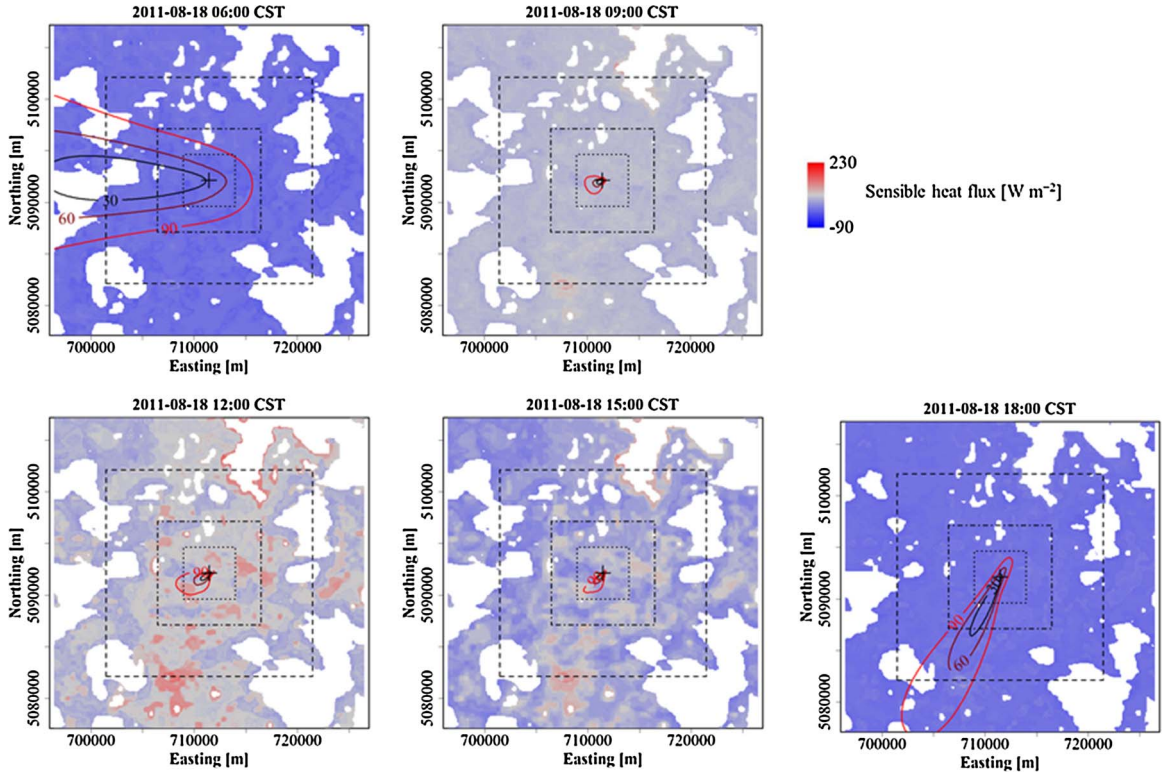

Fig. 8. Flux footprint variations over time at the AmeriFlux Park Falls tall tower at 122 m measurement height, modified after Metzger et al. (2013b). The footprints are superimposed over the ERF derived grids of turbulent sensible heat flux at the lid of the Eulerian control volume.

ensembling for extracting the net low frequency flux contribution from the compensation fluxes perceived as advection error at single tower EC sites. The centerpiece for this functionality is for ERF-VCV to act as 4-D mapping operator: Process understanding and observational information are catalyzed through a combination a systematic extraction and projection leveraging artificial intelligence.

3.1.1. Resilience to external advection errors

Consider the EC vertical flux measurement height as fundamental distance unit, horizontal and vertical. It also intersects with the lid of the Eulerian control volume into which ERF-VCV is projecting (Fig. 2). Per definition of a cumulative footprint weight of unity, the standard EC tower measurements of storage and vertical fluxes each represent a single censused unit. Here, a censused unit represents constrained surfaces, i.e. grid cells with fully explained storage and vertical flux. In reality, the cumulative footprint weight does not origin only from the tower grid cell, but also from further upwind following a 2-D distribution function. Nevertheless, the cumulative footprint weight and corresponding information content remains unity: The tower measurement represents a single fully censused unit consisting of a varying number of fractionally censused units. For the sake of a conservative argument I assume that over time the Lagrangian tower footprint can represent a Eulerian control volume of 10 distance units side length. This approximates the extent of well-constrained footprints under daytime conditions, and results in ~100 censused units. ERF-VCV on the other hand acts as a transfer function, mapping within the range of observed state-space combinations. For a single tower this permits mapping with ≥90% coverage across an Eulerian control volume of side length 50–200 distance units (Xu et al., 2017), resulting in ~10,000 censused units.

Next, the non-censused units or unconstrained surfaces with regard to advection errors are examined: Advection with external can occur through the side walls of the control volume, for which also ERF-VCV does not currently provide boundary conditions. 4 walls of distance unit height result in ~40 non-censused units and ~400 non-censused units for the EC tower and ERF-VCV, respectively. The resilience against external advection can now be approximated as the ratio of censused units to non-censused units, resulting in an absolute resilience of 2.5 and 25 for the EC tower and ERF-VCV, respectively (Fig. 7, red triangles). Hence, ERF-VCV promises to be at least one order of magnitude more resilient to external advection errors compared to an individual EC tower. It can also be seen that the resilience increases directly proportional to the side length of the ERF-VCV target domain (Fig. 7, blue circles), highlighting the importance on EC tower location and driver selection to maximize the projectable area.

3.1.2. Resilience to internal advection errors

ERF-VCV makes use of increasing the control volume so internal net horizontal advection cancels and the compensatory fluxes in the storage and vertical terms trend towards their ensemble value, i.e. their net low frequency contribution (Section 2.3.2). The resilience to internal advection errors can thus be expressed as $\frac{1}{se} \propto 2L$. Here, the standard error $se \propto \frac{1}{\sqrt{N}}$ represents the closeness of the ensemble mean to the true net low frequency flux, with the number of considered grid cells $N \propto 4\,L^2$, and side the length of the Eulerian control volume $2L$. During actual application, ERF-VCV can encounter time-space locations that cannot be projected into as at least one driver exceeds the range of the training data (white spaces in Fig. 8). The extent of the control volume is chosen so that the fraction of white cells is < 10%, thus reducing the resilience of ERV-VCV to internal advection errors by no more than 5%. To summarize: Even if the flux observations informing ERF-VCV are imperfect, the resilience to external and internal advection both increases directly proportional to the control volume side length, by at least one order of magnitude. This effect is further illustrated and discussed in the following.

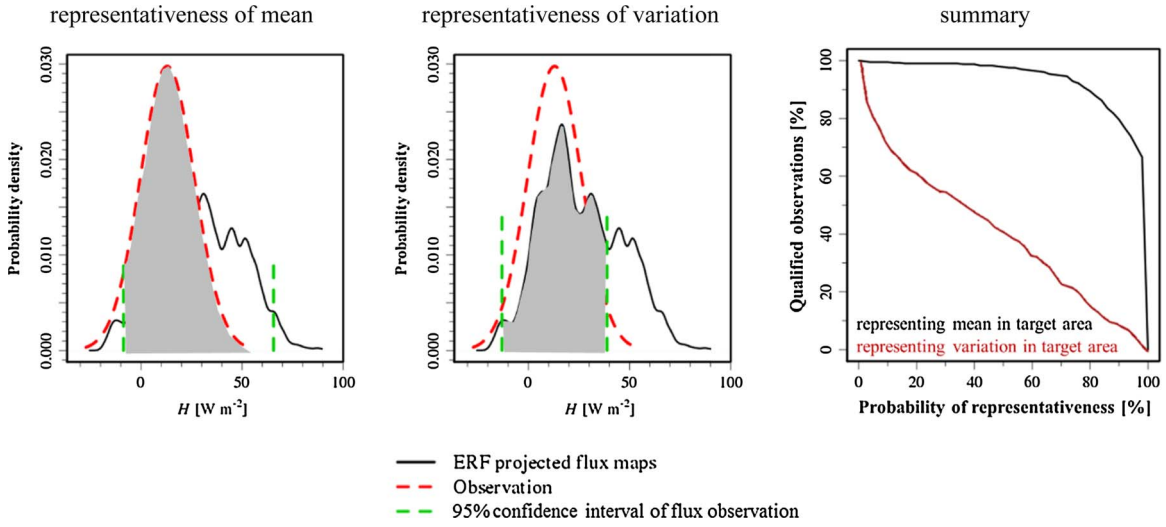

Fig. 9. Left and center panels: Probability density functions of tower observed and ERF projected turbulent sensible heat flux at the WLEF AmeriFlux Park Falls tall tower at 122 m measurement height modified after Xu et al. (2014). ERF projection at the lid of the Eulerian control volume covers a 30 × 30 km target domain. The grey areas indicate, respectively, the probability of the tower-observed flux being representative of the areal mean flux (left panel, 94%), and of the flux variation across the area (center panel, 69%), at a 5% significance level. The right panel shows a summary of these probabilities for July and August 2011.

3.2. Representation, representativeness and energy imbalance

One fundamental challenge for model-data comparison lies in the scale mismatch: EC tower observations represent temporally varying and small source areas (10^0–10^1 km^2) in conjunction with their Lagrangian control volumes (Fig. 3). In contrast, model simulations produce regular, regional-scale grids (10^2–10^3 km^2), much alike the Eulerian control volume (Fig. 6). Here, the ERF methodology provides a promising link through unveiling the regional flux field underlying the footprint-biased observations. Metzger et al. (2014) and Xu et al. (2014) successfully implemented the ERF procedure for the Ameriflux WLEF tall tower based on turbulent flux and downscaled MODIS remote sensing data. The ERF outputs are spatio-temporally explicit projections of the turbulent flux (Fig. 8), and the spatial coverage increases to ≥80% at 25 km^2, ≥60% at 100 km^2, and ≥50% at 400 km^2 (Metzger et al., 2013b; Xu et al., 2017). This demonstrates how model grid cell heat flux can have significant differences and variability from the individual tower measurement.

To address the challenge of spatial scaling to model grid cell the probability of point-to-area representativeness of a tower flux measurement was assessed following Nappo et al. (1982). This was performed not only for the average flux, but also for its variation across a target domain (Fig. 9, left and center panels). The latter is of particular interest, as many boundary layer processes such as mesoscale structures are highly non-linear, and only a small fraction of the tower observations appear to represent the true spatial variability. These processes are suspected to contribute to the observed non-closure of the energy balance (Stoy et al., 2013), which is further addressed below. In model-data fusion, spatial representativeness can serve as a criterion for the selection of observations. In addition, ERF provides an unprecedented advantage compared to existing strategies for model-data fusion: Not only is the expected value quantified, but the entire probability density function over a target domain.

In this way ERF-VCV also overcomes the drawbacks that heterogeneity within the flux footprint imposes on the interpretation of seasonal, annual, and inter-annual *NSAE*: The flux tower footprint can be quite variable between years, and one surface type is likely observed more frequently in one year than in another. Hence, any observed dynamics or potential seasonal trends, as well as any constructed budgets may be quite different only because of sampling a different source area each year (e.g., Griebel et al., 2016; Montaldo and Oren, 2016; Morin et al., 2017). The ERF-VCV's fixed-frame representation across a time-invariant target domain accounts for such variable footprint coverage: Each surface type is now contributing in equitable proportions to the *NSAE*. This allows deciphering true dynamics within each target domain that is unbiased by the fragmented footprint coverage of the flux tower.

ERF-VCV further permits reconciling two principal sources in the problem of energy balance non-closure: "Storage flux" (Leuning et al., 2012) and "spatial heterogeneity" (Foken et al., 2011; Mauder et al., 2007; Stoy et al., 2013). This is achieved through explicitly addressing all terms in the continuity Eq. (5), and by spatially integrating over a temporally consistent target domain.

Storage flux has been shown to contribute to some of this closure due to a lack of suitable observations below the vertical flux measurement height (Leuning et al., 2012). Specifically in the case of tall towers, storage can comprise a substantial amount of the actual surface-atmosphere exchange. This is directly addressed by the ERF-VCV storage flux projection, and the results are 3-D storage time-sequences (Fig. 5 in Xu et al., this issue). Through superposition with the ERF-projected turbulent flux maps at the lid of the Eulerian control volume, the accuracy of surface-atmosphere exchange mapping in representing Eq. (1) is substantially improved (Fig. 10). When aggregated for August 2011 over 400 km^2 centered around the WLEF tower, the storage flux of sensible heat differed in both sign and magnitude by +2.7 W/m^2 between ERF-VCV (2.4 W/m^2) and direct observations (−0.3 W/m^2). The difference was even larger for the corresponding vertical flux (+4.7 W/m^2 or +24%) and the net surface flux (+7.3 W/m^2 or +40%), respectively.

The systematic and significant increase in net sensible heat flux implies improved energy balance closure, and can be explained by the cancellation of advective errors and inclusion of the net low-frequency flux: In the presence of daytime mesoscale structures, strong convection of warmer/wetter air occurs in spatially confined updraft zones. This is accompanied by a slight subsidence of cooler/dryer air across the majority of the target domain, and horizontal compensatory flows between convection and subsidence zones (Kanda et al., 2004). Standard EC from a single tower is not capable of capturing the net low-frequency flux contributions of these boundary layer features, and thus likely cannot represent the areal average surface flux. This is particularly evident from Fig. 9 (left and center panels), where ERF-VCV reproduces the long-tailed spatial distribution of large sensible heat fluxes, which is absent from the corresponding tower observation.

In contrast to a single flux tower with transient Lagrangian

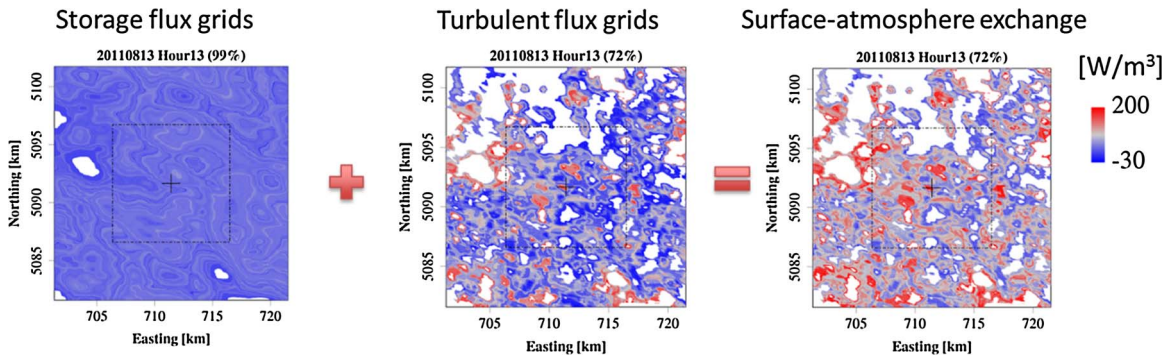

Fig. 10. Projected sensible heat flux grids of storage term (left panel), turbulent (center panel) and net surface-atmosphere exchange (right panel) after Xu et al. (2015). Display is for August 13th, 2011, 13:00–14:00 CST with a tower-centered 20 × 20 km^2 target region. White areas are gaps that cannot be reproduced by ERF because their biophysical properties exceed the range of the training dataset.

footprints and control volumes, ERF-VCV continuously provides the spatial patterning of the total flux across a consistent Eulerian control volume. Spatial ensembling then permits to cancel transient compensation fluxes related to advection. A systematic increase of the target domain heat flux is expected, resulting from the inclusion of the remaining net low-frequency flux. Specifically, Fig. 8 in Xu et al. (this issue) demonstrates for the WLEF AmeriFlux Park Falls tall tower how the net surface fluxes of sensible and latent heat converge to their area-average mean value for a control volume side length of 10 km and 15 km, respectively. This is accompanied by initially erratic behavior at smaller side lengths, as expected from aggregating over an increasing number of mesoscale structures, ultimately leading to a flux increase of 21% and 3%, respectively. The finding is in line with the analytical considerations regarding external and internal resilience to advection errors (Sections 3.1.1 and 3.1.2), which, given a measurement height of 122 m, predict a 10–15-fold improvement.

Spatial heterogeneity is associated with mesoscale variation in net radiation, canopy development, variation in standing water for wetlands, and presence or absence of mesoscale turbulent structures in the atmosphere. The ERF-VCV net surface flux maps can be further analyzed e.g. for variability in surface energy partitioning of sensible and latent heat across space and time.

Observing a spatial phenomenon such as the net surface flux in a fixed location over time assumes ergodicity, and thus homogeneity and stationarity. Field experiments frequently invalidate these assumptions, e.g. through scale analysis (Higgins et al., 2012; Sayde et al., 2015) and spatial statistics (Engelmann and Bernhofer, 2016; Mauder et al., 2008). Here, ERF-VCV comes to the aid and effectively enables spatial EC from a single tower. This is not only easier to routinely operate and cheaper compared to a tower array, but ERF-VCV in addition considers storage flux and thus also removes the assumption of strict stationarity.

3.3. Practical difficulties and proposed solutions

The standard EC technique from a single tower employs strong assumptions on horizontal homogeneity and stationarity in order to reflect the net surface flux. While ERF-VCV does not completely eradicate these assumptions, as shown in Section 2.3.2 it permits to relax them to a large extent. In fact, the resilience to advection errors increases directly proportional to the target domain size, as is shown in Section 3.1.

3.3.1. Assumptions

Nevertheless, ERF-VCV is not free of assumptions. First of all, in order to determine the true surface flux it needs to be assumed that the observations are free of instrument biases (Frank et al., 2013; Fratini et al., 2014; Horst et al., 2015; Kochendorfer et al., 2013; Mauder, 2013). This includes correction of sensor representation errors, such as e.g. when measuring on a slope (Metzger et al., 2015; Serrano-Ortiz et al., 2016).

ERF-VCV then requires the assimilated observations to be dominated by surface flux and not entrainment. This is achieved by filtering both, storage and vertical flux observations for connectivity with the surface using turbulent mixing tests, such as integral turbulence characteristics (Foken, 2017). In result, typically a larger number of nighttime than of daytime observations is discarded, which can result in problematic nighttime data coverage.

Next, ERF-VCV assumes that the relevant combinations of atmospheric dynamics and surface states across the target domain have been sampled by the tower at some point during the observation period. In very complex terrain a single tower might not be sufficient to fulfill this assumption. Fortunately, ERF-VCV permits using driver and response observations from multiple horizontally and vertically distributed platforms together. In fact, e.g. the addition of sub-canopy towers allows investigating the asynchronicity between processes in different ecosystem stories and potentially their partitioning, or high-resolution LIDAR can be utilized to explain topography-induced katabatic flows.

ERF-VCV further assumes that the footprint model is capable of at least partially relating low-frequency fluxes to their surface sources. For this purpose it is principally possible but computationally expensive to explicitly consider non-homogeneous turbulence (Stein et al., 2015; Stohl et al., 2005). However, Xu et al. (2017) and Metzger et al. (2013a) determined that the use of a simple footprint parameterization is not currently limiting ERF-VCV performance.

Lastly, like any inverse technique, ERF-VCV assumes that suitable optimality and performance criteria are being used. The spatio-temporal coverage of the projections provides a first line of defense indicating whether atmospheric dynamics and surface states have been adequately sampled: ERF-VCV can only project into areas with state-space combination that have been experienced by the tower. Next, stratified cross-validation, regression analysis and a bottom-up uncertainty budget quantify how well ERF-VCV can reproduce dependent and independent subsets of tower flux observations. Lastly, inter-site comparison in combination with a top-down uncertainty budget (Xu et al., 2017) provides the ultimate assessment tool. Uncertainty propagation, bootstrapping as well as cross-site validation agree on the ERF methods' accuracy on the order of 10%, i.e. smaller or equal to the EC measurement technique itself (Xu et al., 2017). This represents the bias resulting from ERF's overall analytical sequence, which is compensated via site-specific calibration prior to use of the results. On the other hand, precision (ensemble random error; Mahrt, 1998) rapidly improves with the number of grid cells considered, to order 1% over a 10 × 10 km target domain.

3.3.2. Verification and validation

Initial verification and validation of the ERF vertical flux component has been successful (Metzger et al., 2013a; Xu et al., 2017). However, to warrant general application a thorough validation across ecosystems, climates and tower setups is required, in particular for the ERF-VCV

storage flux component (Xu et al., this issue). To be fully independent such validation should be performed against true spatial flux datasets, which only recently become available with the required density of observations (e.g., Li et al., 2013).

Initially, the theoretical soundness and statistical significance of ERF-VCV can also be tested against synthetic reference datasets from large eddy simulations. Next, the practical applicability of the ERF-VCV spatial rectification can be determined as function of a minimum standard set of drivers for EC sites spanning various eco-climates. ERF-VCV can then be cross-validated at sites with multiple proximate but independent EC towers, including energy balance considerations. Particularly suitable for such validation are proximate EC towers and tower matrices in combination with a hierarchy of observations (tower, flux and remote sensing aircraft, satellite). This more than likely would require the design of a suitable energy balance closure experiment.

Even in the presence of such experiment, spatio-temporally explicit information on net radiation and soil heat flux will be challenging to get by. Here it can be explored to expand the ERF methodology to net radiation and soil heat flux, in order to evaluate energy balance closure with consistent spatial representation of all contributing terms.

4. Summary and conclusions

Even from a single eddy-covariance tower, the environmental response function virtual control volume (ERF-VCV) methodology reduces the reliance on crucial mass balance simplifications by at least one order of magnitude. In the same process tower location bias is effectively removed. A systematic increase in heat net surface flux was observed and related to the ability of ERF-VCV to include low frequency flux contributions while being resilient to advective errors. This promises improved energy balance closure, which may also have implications for other trace gas fluxes such as CO_2 (Foken, 2008).

This is achieved through a combination of spectral averaging, source area modeling and spatio-temporally explicit ensembling using machine learning: ERF-VCV effectively acts as a 4-D spatio-temporal data assimilation system which explicitly addresses each term in the continuity equation. In this way ERF-VCV is extensible and can incorporate additional observational and mechanistic constraints, neither of which requiring spatio-temporal regularity or continuity. Examples are multiple eddy-covariance towers and aircraft, distributed temperature sensing, LIDAR and satellite remote sensing or even meteorological re-analysis. Through maximizing data use efficiency ERF-VCV can guide efficient and effective experiment design, and thus maximize return on investment. It should be noted that ERF-VCV does not depend on a given set of measurements, but rather acts as a flexible catalyst on however much information is available. This makes it generally applicable across a broader range of disciplines, such as “machine learning for Geosciences”.

The results of ERF-VCV are high-dimensional response functions and net surface flux fields that can be used for the assessment and study of environmental relationships and their spatio-temporal patterning and aggregation. Application examples are the regionalization of energy and carbon fluxes from aircraft and tower (Metzger et al., 2013a; Xu et al., 2017), spatially explicit mapping of biogenic and geogenic CH_4 sources in the Arctic (Kohnert et al., 2017; Sachs et al., 2014), or the attribution of anthropogenic NO_x and VOC emissions (Vaughan et al., 2016; Vaughan et al., 2017).

ERF-VCV provides a rectifying observational operator for unbiased model-data fusion, and process representation at the model grid scale: In-situ co-varying processes are extracted on the field/landscape-scale and can be used to systematically inform model structure, in addition to parameterizing, initializing, constraining and validating models and inventories with the net surface flux fields. This permits the identification of key drivers, responses and the governing in situ processes, and substantially improves our ability to study scale-dependent questions such as microclimate adaptation, water use efficiency or impact of land-use and land cover.

Ultimately, ERF-VCV attains a fixed-frame, thus equitable and time-invariant representation of the net surface-atmosphere exchange across a target domain. This permits adequately capturing true environmental behavior, as well as the unbiased utilization of e.g. energy, water and carbon cycle observations in model-data comparison, assimilation, and process representation at model grid scale.

Acknowledgements

This work has arisen out of and profited from insightful discussions with many individuals at conferences, during proposal writing and in coding sessions. In particular I would like to acknowledge the constructive criticism from and collaborative work with Ankur Desai and Ke Xu (University of Wisconsin, Madison, USA), and Cove Sturtevant, David Durden, and Natchaya Pingintha-Durden (National Ecological Observatory Network, Battelle, Boulder, USA).

The National Ecological Observatory Network is a project sponsored by the National Science Foundation and managed under cooperative agreement by Battelle Ecology, Inc. This material is based upon work supported by the National Science Foundation [grant DBI-0752017]. Any opinions, findings, and conclusions or recommendations expressed in this material are those of the author and do not necessarily reflect the views of the National Science Foundation.

References

Anderson, M.C., et al., 2008. A thermal-based remote sensing technique for routine mapping of land-surface carbon, water and energy fluxes from field to regional scales. Remote Sens. Environ. 112 (12), 4227–4241.
Aubinet, M., Feigenwinter, C., 2010. Direct CO_2 advection measurements and the night flux problem. Agric. For. Meteorol. 150 (5), 651–654.
Baldocchi, D., 2008. ‘Breathing’ of the terrestrial biosphere: lessons learned from a global network of carbon dioxide flux measurement systems. Aust. J. Bot. 56 (1), 1–26.
Barnhart, B.L., Eichinger, W.E., Prueger, J.H., 2012. Introducing an Ogive method for discontinuous data. Agric. For. Meteorol. 162–163, 58–62.
Barr, A.G., et al., 2013. Use of change-point detection for friction–velocity threshold evaluation in eddy-covariance studies. Agric. For. Meteorol. 171–172, 31–45.
Beer, C., et al., 2010. Terrestrial gross carbon dioxide uptake: global distribution and covariation with climate. Science 329 (5993), 834–838.
Bertoldi, G., Kustas, W., Albertson, J., 2013. Evaluating source area contributions from aircraft flux measurements over heterogeneous land using large-eddy simulation. Boundary Layer Meteorol. 147 (2), 261–279.
Beyrich, F., et al., 2006. Area-averaged surface fluxes over the LITFASS region based on eddy-covariance measurements. Boundary Layer Meteorol. 121 (1), 33–65.
Bjorkegren, A.B., Grimmond, C.S.B., Kotthaus, S., Malamud, B.D., 2015. CO_2 emission estimation in the urban environment: measurement of the CO_2 storage term. Atmos. Environ. 122, 775–790.
Cammalleri, C., et al., 2012. Applications of a remote sensing-based two-source energy balance algorithm for mapping surface fluxes without in situ air temperature observations. Remote Sens. Environ. 124, 502–515.
Carvalhais, N., et al., 2014. Global covariation of carbon turnover times with climate in terrestrial ecosystems. Nature 514 (7521), 213–217.
Charuchittipan, D., Babel, W., Mauder, M., Leps, J.-P., Foken, T., 2014. Extension of the averaging time in eddy-covariance measurements and its effect on the energy balance closure. Boundary-Layer Meteorol. 152 (3), 303–327.
Chen, J.M., Leblanc, S.G., Cihlar, J., Desjardins, R.L., MacPherson, J.I., 1999. Extending aircraft- and tower-based CO_2 flux measurements to a boreal region using a Landsat thematic mapper land cover map. J. Geophys. Res. [Atmos.] 104 (D14), 16859–16877.
Chen, B., et al., 2010. A data-model fusion approach for upscaling gross ecosystem productivity to the landscape scale based on remote sensing and flux footprint modelling. Biogeosciences 7 (9), 2943–2958.
Chen, B., et al., 2011. Assessing eddy-covariance flux tower location bias across the Fluxnet-Canada Research Network based on remote sensing and footprint modelling. Agric. For. Meteorol. 151 (1), 87–100.
Chen, B., et al., 2012. Characterizing spatial representativeness of flux tower eddy-covariance measurements across the Canadian Carbon Program Network using remote sensing and footprint analysis. Remote Sens. Environ. 124, 742–755.
Desai, A.R., et al., 2008. Influence of vegetation and seasonal forcing on carbon dioxide fluxes across the Upper Midwest, USA: implications for regional scaling. Agric. For. Meteorol. 148 (2), 288–308.
Desai, A.R., Helliker, B.R., Moorcroft, P.R., Andrews, A.E., Berry, J.A., 2010. Climatic controls of interannual variability in regional carbon fluxes from top-down and bottom-up perspectives. J. Geophys. Res.: Biogeosci. 115 (G2).
Desai, A.R., et al., 2016. How many flux towers are enough? Energy balance closure and large eddy simulation as diagnostic tools for secondary circulations. In: 32nd

Conference on Agricultural and Forest Meteorology. Salt Lake City, U.S.A.
Desjardins, R.L., MacPherson, J.I., Schuepp, P.H., Karanja, F., 1989. An evaluation of aircraft flux measurements of CO_2, water vapor and sensible heat. Boundary Layer Meteorol. 47 (1), 55–69.
Elith, J., Leathwick, J.R., Hastie, T., 2008. A working guide to boosted regression trees. J. Anim. Ecol. 77 (4), 802–813.
Engelmann, C., Bernhofer, C., 2016. Exploring eddy-covariance measurements using a spatial approach: the eddy matrix. Boundary Layer Meteorol. 161 (1), 1–17.
Ershadi, A., McCabe, M.F., Evans, J.P., Walker, J.P., 2013. Effects of spatial aggregation on the multi-scale estimation of evapotranspiration. Remote Sens. Environ. 131, 51–62.
Finnigan, J.J., Clement, R., Malhi, Y., Leuning, R., Cleugh, H.A., 2003. A re-evaluation of long-term flux measurement techniques. Part 1: averaging and coordinate rotation. Boundary Layer Meteorol. 107 (1), 1–48.
Finnigan, J.J., 2004. A re-evaluation of long-term flux measurement techniques. Part 2: coordinate systems. Boundary Layer Meteorol. 113 (1), 1–41.
Foken, T., Wichura, B., 1996. Tools for quality assessment of surface-based flux measurements. Agric. For. Meteorol. 78 (1–2), 83–105.
Foken, T., et al., 2004. Post-field data quality conirol. In: Lee, X., Law, B., Massman, W. (Eds.), Handbook of Micrometeorology: A Guide for Surface Flux Measurement and Analysis. Springer, Dordrecht, pp. 181–208.
Foken, T., 2008. The energy balance closure problem: an overview. Ecol. Appl. 18 (6), 1351–1367.
Foken, T., et al., 2010. Energy balance closure for the LITFASS-2003 experiment. Theor. Appl. Climatol. 101 (1–2), 149–160.
Foken, T., et al., 2011. Results of a panel discussion about the energy balance closure correction for trace gases. Bull. Am. Meteorol. Soc. 92 (4), ES13–ES18.
Foken, T., 2017. Micrometeorology. Springer, Berlin, Heidelberg 360 pp.
Frank, J.M., Massman, W.J., Ewers, B.E., 2013. Underestimates of sensible heat flux due to vertical velocity measurement errors in non-orthogonal sonic anemometers. Agric. For. Meteorol. 171–172, 72–81.
Fratini, G., McDermitt, D.K., Papale, D., 2014. Eddy-covariance flux errors due to biases in gas concentration measurements: origins, quantification and correction. Biogeosciences 11 (4), 1037–1051.
Griebel, A., et al., 2016. Effects of inhomogeneities within the flux footprint on the interpretation of seasonal, annual, and interannual ecosystem carbon exchange. Agric. For. Meteorol. 221, 50–60.
Hayhoe, K., et al., 2006. Past and future changes in climate and hydrological indicators in the US Northeast. Clim. Dyn. 28 (4), 381–407.
Higgins, C.W., et al., 2012. The effect of scale on the applicability of Taylor's frozen turbulence hypothesis in the atmospheric boundary layer. Boundary Layer Meteorol. 143 (2), 379–391.
Horst, T.W., Semmer, S.R., Maclean, G., 2015. Correction of a non-orthogonal, three-component sonic anemometer for flow distortion by transducer shadowing. Boundary Layer Meteorol. 1–25.
Hulme, M., Osborn, T.J., Johns, T.C., 1998. Precipitation sensitivity to global warming: comparison of observations with HadCM2 simulations. Geophys. Res. Lett. 25 (17), 3379–3382.
Huntington, T.G., 2006. Evidence for intensification of the global water cycle: review and synthesis. J. Hydrol. 319 (1–4), 83–95.
IPCC, 2013. Climate Change 2013 – The Physical Science Basis, Contribution of Working Group 1 to the Fifth Assessment Report of the Intergovernmental Panel on Climate Change. Intergovernmental Panel on Climate Change, Cambridge, United Kingdom.
Kanda, M., Inagaki, A., Letzel, M.O., Raasch, S., Watanabe, T., 2004. LES study of the energy imbalance problem with Eddy covariance fluxes. Boundary Layer Meteorol. 110 (3), 381–404.
Kljun, N., Calanca, P., Rotach, M.W., Schmid, H.P., 2004. A simple parameterisation for flux footprint predictions. Boundary Layer Meteorol. 112 (3), 503–523.
Kljun, N., Calanca, P., Rotach, M.W., Schmid, H.P., 2015. A simple two-dimensional parameterisation for flux footprint prediction (FFP). Geosci. Model Dev. 8 (11), 3695–3713.
Kochendorfer, J., Meyers, T., Frank, J., Massman, W., Heuer, M., 2013. Reply to the comment by Mauder on how well can we measure the vertical wind speed? Implications for fluxes of energy and mass. Boundary Layer Meteorol. 147 (2), 337–345.
Kohnert, K., Serafimovich, A., Metzger, S., Hartmann, J., Sachs, T., 2017. Strong geologic methane emissions from discontinuous terrestrial permafrost in the Mackenzie Delta, Canada. Scientific Reports 7 (1), 5828.
Leclerc, M.Y., Foken, T., 2014. Footprints in Micrometeorology and Ecology. Springer, Berlin, Heidelberg, Germany 239 pp.
Leuning, R., van Gorsel, E., Massman, W.J., Isaac, P.R., 2012. Reflections on the surface energy imbalance problem. Agric. For. Meteorol. 156, 65–74.
Li, X., et al., 2013. Heihe watershed allied telemetry experimental research (HiWATER): scientific objectives and experimental design. Bull. Am. Meteorol. Soc. 94 (8), 1145–1160.
Lindroth, A., Mölder, M., Lagergren, F., 2010. Heat storage in forest biomass improves energy balance closure. Biogeosciences 7 (1), 301–313.
Liu, S.M., et al., 2011. A comparison of eddy-covariance and large aperture scintillometer measurements with respect to the energy balance closure problem. Hydrol. Earth Syst. Sci. 15 (4), 1291–1306.
Luyssaert, S., et al., 2008. Old-growth forests as global carbon sinks. Nature 455 (7210), 213–215.
Mahrt, L., 1996. The bulk aerodynamic formulation over heterogeneous surfaces. Boundary Layer Meteorol. 78 (1-2), 87–119.
Mahrt, L., 1998. Flux sampling errors for aircraft and towers. J. Atmos. Oceanic Technol. 15 (2), 416–429.
Mahrt, L., 2000. Surface heterogeneity and vertical structure of the boundary layer. Boundary Layer Meteorol. 96 (1), 33–62.
Markkanen, T., Steinfeld, G., Kljun, N., Raasch, S., Foken, T., 2010. A numerical case study on footprint model performance under inhomogeneous flow conditions. Meteorologische Zeitschrift 19 (6), 539–547.
Mason, P.J., 1988. The formation of areally-averaged roughness lengths. Q. J. R. Meteorolog. Soc. 114 (480), 399–420.
Mauder, M., Foken, T., 2006. Impact of post-field data processing on eddy covariance flux estimates and energy balance closure. Meteorologische Zeitschrift 15 (6), 597–609.
Mauder, M., Jegede, O.O., Okogbue, E.C., Wimmer, F., Foken, T., 2007. Surface energy balance measurements at a tropical site in West Africa during the transition from dry to wet season. Theor. Appl. Climatol. 89 (3), 171–183.
Mauder, M., Desjardins, R.L., Pattey, E., Gao, Z., van Haarlem, R., 2008. Measurement of the sensible eddy heat flux based on spatial averaging of continuous ground-based observations. Boundary Layer Meteorol. 128 (1), 151–172.
Mauder, M., et al., 2013. A strategy for quality and uncertainty assessment of long-term eddy-covariance measurements. Agric. For. Meteorol. 169, 122–135.
Mauder, M., 2013. A comment on How well can we measure the vertical wind speed? Implications for fluxes of energy and mass by Kochendorfer et al. Boundary Layer Meteorol. 147 (2), 329–335.
Mengelkamp, H.T., et al., 2006. Evaporation over a heterogeneous land surface – the EVA-GRIPS project. Bull. Am. Meteorol. Soc. 87 (6), 775–786.
Metzger, S., et al., 2012. Eddy-covariance flux measurements with a weight-shift micro-light aircraft. Atmos. Meas. Tech. 5 (7), 1699–1717.
Metzger, S., et al., 2013a. Spatially explicit regionalization of airborne flux measurements using environmental response functions. Biogeosciences 10 (4), 2193–2217.
Metzger, S., et al., 2013b. Spatio-temporal rectification of tower-based eddy-covariance flux measurements for consistently informing process-based models. In: 46th AGU Annual Fall Meeting. San Francisco, U.S.A.
Metzger, S., et al., 2014. Mapping the flux field around eddy-covariance measurements. In: 31st AMS Conference on Agricultural and Forest Meteorology. Portland, U.S.A.
Metzger, S., et al., 2015. Alignment of surface-atmosphere exchange sensors at sloped sites: an integrated strategy. In: 48th AGU Annual Fall Meeting. San Francisco, U.S.A.
Metzger, S., et al., 2017. eddy4R 0. 2. 0: a DevOps model for community-extensible processing and analysis of eddy-covariance data based on R, Git, Docker, and HDF5. Geosci. Model Dev. 10 (9), 3189–3206.
Montaldo, N., Oren, R., 2016. The way the wind blows matters to ecosystem water use efficiency. Agric. For. Meteorol. 217, 1–9.
Morin, T.H., et al., 2017. Combining eddy-covariance and chamber measurements to determine the methane budget from a small, heterogeneous urban floodplain wetland park. Agric. For. Meteorol. 237–238, 160–170.
Nappo, C.J., et al., 1982. The workshop on the representativeness of meteorological observations June 1981, Boulder, Colorado. Bull. Am. Meteorol. Soc. 63 (7), 761–764.
National Academy of Sciences, 2013. Abrupt Impacts of Climate Change: Anticipating Surprises (prepublication Copy). National Academy of Sciences, Washington D.C, U.S.A.
Oncley, S.P., et al., 2007. The energy balance experiment EBEX-2000. Part I: overview and energy balance. Boundary Layer Meteorol. 123 (1), 1–28.
Panin, G.N., Tetzlaff, G., Raabe, A., 1998. Inhomogeneity of the land surface and problems in the parameterization of surface fluxes in natural conditions. Theor. Appl. Climatol. 60 (1), 163–178.
R Core Team, 2016. R: A Language and Environment for Statistical Computing. R Foundation for Statistical Computing, Vienna, Austria.
Rannik, Ü., et al., 2012. Footprint analysis. In: Aubinet, M., Vesala, T., Papale, D. (Eds.), Eddy Covariance: A Practical Guide to Measurement and Data Analysis. Springer, Dordrecht, Heidelberg, London, New York, pp. 211–261.
Raupach, M.R., 1988. Canopy transport processes. In: Steffen, W.L., Denmead, O.T. (Eds.), Flow and Transport in the Natural Environment. Springer, Berlin, pp. 95–127.
Sachs, T., Serafimovich, A., Metzger, S., Kohnert, K., Hartmann, J., 2014. Low permafrost methane emissions from arctic airborne flux measurements. In: 47th AGU Annual Fall Meeting. San Francisco, U.S.A.
Sayde, C., Thomas, C.K., Wagner, J., Selker, J., 2015. High-resolution wind speed measurements using actively heated fiber optics. Geophys. Res. Lett. 42 (22) 10,064–10,073.
Schaller, C., Göckede, M., Foken, T., 2017. Flux calculation of short turbulent events – comparison of three methods. Atmos. Meas. Tech. 10 (3), 869–880.
Schmid, H.P., Lloyd, C.R., 1999. Spatial representativeness and the location bias of flux footprints over inhomogeneous areas. Agric. For. Meteorol. 93 (3), 195–209.
Schmid, H.P., 2002. Footprint modeling for vegetation atmosphere exchange studies: a review and perspective. Agric. For. Meteorol. 113 (1–4), 159–183.
Serrano-Ortiz, P., et al., 2015. Surface-parallel sensor orientation for assessing energy balance components on mountain slopes. Boundary-Layer Meteorol. 158 (3), 489–499.
Stein, A.F., et al., 2015. NOAA's HYSPLIT atmospheric transport and dispersion modeling system. Bull. Am. Meteorol. Soc. 96 (12), 2059–2077.
Steinfeld, G., Letzel, M.O., Raasch, S., Kanda, M., Inagaki, A., 2007. Spatial representativeness of single tower measurements and the imbalance problem with eddy-covariance fluxes: results of a large-eddy simulation study. Boundary Layer Meteorol. 123 (1), 77–98.
Stohl, A., Forster, C., Frank, A., Seibert, P., Wotawa, G., 2005. Technical note: the

lagrangian particle dispersion model FLEXPART version 6.2. Atmos. Chem. Phys. 5 (9), 2461–2474.
Stoy, P.C., et al., 2009. Using information theory to determine optimum pixel size and shape for ecological studies: aggregating land surface characteristics in arctic ecosystems. Ecosystems 12 (4), 574–589.
Stoy, P.C., et al., 2013. A data-driven analysis of energy balance closure across FLUXNET research sites: the role of landscape scale heterogeneity. Agric. For. Meteorol. 171–172, 137–152.
Strunin, M.A., Hiyama, T., 2004. Applying wavelet transforms to analyse aircraft-measured turbulence and turbulent fluxes in the atmospheric boundary layer over eastern Siberia. Hydrol. Processes 18 (16), 3081–3098.
Stull, R.B., 1988. An Introduction to Boundary Layer Meteorology. Kluwer Academic Publishers, Dordrecht, The Netherlands 670 pp.
Taylor, G.I., 1938. The spectrum of turbulence. Proc. R. Soc. Lond. A 164, 476–490.
Thomas, C., Foken, T., 2005. Detection of long-term coherent exchange over spruce forest using wavelet analysis. Theor. Appl. Climatol. 80 (2), 91–104.
van den Kroonenberg, A., Bange, J., 2007. Turbulent flux calculation in the polar stable boundary layer: multiresolution flux decomposition and wavelet analysis. J. Geophys. Res. [Atmos.] 112 (D6).
Vaughan, A.R., et al., 2016. Spatially resolved flux measurements of NOx from London suggest significantly higher emissions than predicted by inventories. Faraday Discuss. 189, 455–472.
Vaughan, A.R., et al., 2017. VOC emission rates over London and South East England obtained by airborne eddy covariance. Faraday Discuss. 200, 599–620.
Vesala, T., et al., 2008. Flux and concentration footprint modelling: state of the art. Environ. Pollut. 152 (3), 653–666.
Wang, W., Davis, K.J., Cook, B.D., Butler, M.P., Ricciuto, D.M., 2006. Decomposing CO_2 fluxes measured over a mixed ecosystem at a tall tower and extending to a region: a case study. J. Geophys. Res.: Biogeosci. 111 (G2).
Wilson, K., et al., 2002. Energy balance closure at FLUXNET sites. Agric. Forest Meteorol. 113 (1–4), 223–243.
Xiao, J.F., Davis, K.J., Urban, N.M., Keller, K., Saliendra, N.Z., 2011. Upscaling carbon fluxes from towers to the regional scale: influence of parameter variability and land cover representation on regional flux estimates. J. Geophys. Res. Biogeosci. 116.
Xu, K., Metzger, S., Kljun, N., Taylor, J.R., Desai, A.R., 2014. How to consistently inform NEON's land surface model with tower-based eddy covariance flux observations? A novel approach to spatio-temporal rectification. In: 99th ESA Annual Meeting. Sacramento, U.S.A.
Xu, K., Metzger, S., Desai, A.R., 2015. Mapping surface-atmosphere exchange by using environmental response function for both turbulent and storage eddy-covariance fluxes. In: 48th AGU Annual Fall Meeting. San Francisco, U.S.A.
Xu, K., Metzger, S., Desai, A.R., 2017a. Upscaling tower-observed turbulent exchange at fine spatio-temporal resolution using environmental response functions. Agric. Forest Meteorol. 232, 10–22.
K. Xu, S. Metzger, A.R. Desai, Surface-atmosphere exchange in a box: space-time resolved storage and net vertical fluxes from tower-based eddy covariance. Agric. For. Meteorol (in this issue).
Yi, C., et al., 2010. Climate control of terrestrial carbon exchange across biomes and continents. Environ. Res. Lett. 5 (3), 034007.
Zitouna-Chebbi, R., Prévot, L., Jacob, F., Mougou, R., Voltz, M., 2012. Assessing the consistency of eddy covariance measurements under conditions of sloping topography within a hilly agricultural catchment. Agric. Forest Meteorol. 164, 123–135.